AGU PUBLICATIONS

JGR

Journal of Geophysical Research: Biogeosciences

RESEARCH ARTICLE
10.1002/2014JG002695

Key Points:
- DOM is sensitive to permafrost thaw
- 14C of DOM is closely related to optical properties of DOM
- DOM may serve as tool for detecting thaw

Supporting Information:
- Readme
- Text 01

Correspondence to:
J. A. O'Donnell,
jaodonnell@nps.gov

Citation:
O'Donnell, J. A., G. R. Aiken, M. A. Walvoord, P. A. Raymond, K. D. Butler, M. M. Dornblaser, and K. Heckman (2014), Using dissolved organic matter age and composition to detect permafrost thaw in boreal watersheds of interior Alaska, *J. Geophys. Res. Biogeosci.*, *119*, doi:10.1002/2014JG002695.

Received 16 APR 2014
Accepted 11 OCT 2014
Accepted article online 21 OCT 2014

Using dissolved organic matter age and composition to detect permafrost thaw in boreal watersheds of interior Alaska

Jonathan A. O'Donnell[1], George R. Aiken[2], Michelle A. Walvoord[3], Peter A. Raymond[4], Kenna D. Butler[2], Mark M. Dornblaser[2], and Katherine Heckman[5]

[1]Arctic Network, National Park Service, Fairbanks, Alaska, USA, [2]U.S. Geological Survey, Boulder, Colorado, USA, [3]U.S. Geological Survey, Lakewood, Colorado, USA, [4]Yale School of Forestry and Environmental Studies, New Haven, Connecticut, USA, [5]U.S. Department of Agriculture, Forest Service and Lawrence Livermore National Laboratory, Livermore, California, USA

Abstract Recent warming at high latitudes has accelerated permafrost thaw, which can modify soil carbon dynamics and watershed hydrology. The flux and composition of dissolved organic matter (DOM) from soils to rivers are sensitive to permafrost configuration and its impact on subsurface hydrology and groundwater discharge. Here, we evaluate the utility of DOM composition and age as a tool for detecting permafrost thaw in three rivers (Beaver, Birch, and Hess Creeks) within the discontinuous permafrost zone of interior Alaska. We observed strong temporal controls on $\Delta^{14}C$ content of hydrophobic acid isolates ($\Delta^{14}C$-HPOA) across all rivers, with the most enriched values occurring during spring snowmelt ($75 \pm 8‰$) and most depleted during winter flow ($-21 \pm 8‰$). Radiocarbon ages of winter flow samples ranged from 35 to 445 yr BP, closely tracking estimated median base flow travel times for this region (335 years). During spring snowmelt, young DOM was composed of highly aromatic, high molecular-weight compounds, whereas older DOM of winter flow had lower aromaticity and molecular weight. We observed a significant correlation between $\Delta^{14}C$-HPOA and UV absorbance coefficient at 254 nm (α_{254}) across all study rivers. Using α_{254} as an optical indicator for $\Delta^{14}C$-HPOA, we also observed a long-term decline in α_{254} during maximum annual thaw depth over the last decade at the Hess Creek study site. These findings suggest a shift in watershed hydrology associated with increasing active layer thickness. Further development of DOM optical indicators may serve as a novel and inexpensive tool for detecting permafrost degradation in northern watersheds.

1. Introduction

Soils of the northern permafrost region store large amounts of organic carbon (C) [*Tarnocai et al.*, 2009; *Hugelius et al.*, 2013], a portion of which will likely become destabilized with soil warming and thawing [*Harden et al.*, 2012; *Natali et al.*, 2013]. Recent warming at high latitudes has accelerated rates of permafrost thaw [e.g., *Jorgenson et al.*, 2006], which may drive a permafrost-carbon feedback to the climate system [*Koven et al.*, 2011; *von Deimling et al.*, 2012; *MacDougall et al.*, 2012]. Local conditions, such as post-thaw changes in soil drainage and redox status, govern turnover rates and the forms of C released [*Schuur et al.*, 2008]. Given the global climate and policy implications of this feedback [*Schaefer et al.*, 2012], most research to date on permafrost C has focused on the release of greenhouse gases (carbon dioxide (CO_2), methane (CH_4)) from soils to the atmosphere. However, considerable evidence indicates that permafrost thaw is also driving changes to the lateral flux of C from soils to freshwater and marine ecosystems [*Frey and McClelland*, 2009; *Tank et al.*, 2012; *Vonk et al.*, 2012; *Vonk and Gustafsson*, 2013]. For instance, several studies have associated the flux of aged particulate organic carbon (POC) with thaw-induced erosion of riverbanks [*Guo and Macdonald*, 2006; *Guo et al.*, 2007] and coastlines [*Vonk et al.*, 2012]. The riverine flux of dissolved organic carbon (DOC) is also highly sensitive to permafrost thaw and subsequent changes in watershed hydrology [*Striegl et al.*, 2005; *Frey and Smith*, 2005], although the magnitude and directionality of the response appear to differ regionally across the circumarctic [*Tank et al.*, 2012]. In addition to flux estimates, dissolved organic matter (DOM) composition varies with permafrost state across watersheds in the northern permafrost region [*Balcarczyk et al.*, 2009; *O'Donnell et al.*, 2010, 2012a].

The finding that the flux and composition of DOM are tightly linked to watershed hydrology in temperate systems [*Hornberger et al.*, 1994; *Boyer et al.*, 1997; *Raymond and Saiers*, 2010; *Hanley et al.*, 2013] has more

recently been extended to the northern permafrost region [*Petrone et al*., 2006; *Lyon et al*., 2010; *Laudon et al*., 2011; *Giesler et al*., 2014]. Previous studies in the Yukon River Basin (YRB), Alaska, have documented shifts in DOM composition across seasons and watersheds that differ with source water contributions to river flow [*Striegl et al*., 2007; *Spencer et al*., 2008; *O'Donnell et al*., 2010]. Furthermore, increases in groundwater contribution to discharge associated with recent permafrost thaw [*Walvoord and Striegl*, 2007] can greatly modify DOM composition [*O'Donnell et al*., 2012a] through reductions in aromaticity and the proportion of hydrophobic acids. This shift in DOM composition has important implications for the fate of DOM, including rates of DOM mineralization [*Mann et al*., 2012; *Wickland et al*., 2012], DOM reactivity with mineral soils [*Kalbitz et al*., 2005; *Kawahigashi et al*., 2006], C evasion from inland surface waters to the atmosphere [*Striegl et al*., 2012; *Raymond et al*., 2013], and export from terrestrial to aquatic and marine ecosystems [*McGuire et al*., 2010; *Aufdenkampe et al*., 2011]. Despite many recent advances in permafrost C research, a disconnect still exists between soil organic matter (SOM) and thermal dynamics in terrestrial ecosystems and riverine DOM dynamics, in part due to the inherent complexity of subsurface hydrology in regions of degrading permafrost. Furthermore, DOM sources (e.g., plant- or microbially derived DOC) and sinks (e.g., mineralization, sorption, etc.) within soils of arctic and subarctic watersheds have not been fully characterized through field or experimental studies, limiting model parameterization in process-based simulations [*Fan et al*., 2010; *Kicklighter et al*., 2013].

Radiocarbon ($\Delta^{14}C$) measurements of riverine DOM ($\Delta^{14}C$-DOM or $\Delta^{14}C$-DOC) may serve as a powerful tool for tracking seasonal, inner-annual, and decadal shifts in DOM source and radiocarbon abundance in response to thawing permafrost. A number of studies have measured $\Delta^{14}C$-DOM in high-latitude systems [*Benner et al*., 2004; *Neff et al*., 2006; *Guo and Macdonald*, 2006; *Guo et al*., 2007; *Raymond et al*., 2007; *Striegl et al*., 2007; *Hood et al*., 2009; *Aiken et al*., 2014]. Most of these studies have reported that the annual DOC flux is of modern origin, although $\Delta^{14}C$ values typically decline from snowmelt through the summer-autumn period and into winter flow conditions [e.g., *Neff et al*., 2006]. This temporal trend in $\Delta^{14}C$-DOM in part reflects seasonal thawing of the active layer and vertical distribution of $\Delta^{14}C$ of SOM in watersheds underlain by permafrost. Seasonally frozen ground in the active layer exerts a strong control on the depth and transit time of shallow subsurface flows [*Ge et al*., 2011; *Wellman et al*., 2013]. $\Delta^{14}C$ of SOM is also depth dependent, with modern C in shallow organic soils, and Holocene- and Pleistocene-aged C in near-surface permafrost [*O'Donnell et al*., 2011a; *Hicks Pries et al*., 2012]. The seasonal shift in $\Delta^{14}C$-DOM may also reflect a transition in source-water contribution from shallow supra-permafrost groundwater to deep sub-permafrost groundwater [*Bense et al*., 2009]. Under future climate scenarios, permafrost thaw via increased active layer thickness (ALT) [e.g., *Marchenko et al*., 2008] and reduced spatial coverage [e.g., *Walvoord et al*., 2012] will likely drive increases in the proportion of old DOC in high-latitude rivers. However, some evidence indicates that old DOC released from thawed yedoma (i.e., late-Pleistocene ice- and organic-rich silt) is highly labile [*Vonk et al*. 2013] and may be susceptible to rapid mineralization and loss prior to reaching large downstream rivers.

The goal of this study was to examine spatial and temporal patterns of $\Delta^{14}C$-DOM and composition in three tributaries of the Yukon River (Beaver Creek, Birch Creek, and Hess Creek), and to evaluate the utility of DOM optical measurements as a means of detecting watershed-scale permafrost thaw. To pursue these goals, we (1) measured $\Delta^{14}C$ of hydrophobic acid (HPOA) isolates and bulk DOC during spring snowmelt, summer-autumn flow, and winter flow, (2) compared $\Delta^{14}C$ with optical measurements of DOM composition, and (3) examined long-term trends in DOM composition at maximum annual thaw depth. We used HPOA isolates for $\Delta^{14}C$ analysis for several key reasons. First, we were able to take advantage of archived solid-phase HPOA isolates as a means of reconstructing past trends in DOM age over time. Second, methods for measuring $\Delta^{14}C$ on bulk DOC are complex and not readily available in most labs. Third, while the HPOA is typically the dominant fraction in these systems [*O'Donnell et al*., 2010], it also varies considerably across different DOC concentrations. To evaluate the broader utility of $\Delta^{14}C$-HPOA, we evaluate the relationship between $\Delta^{14}C$ of bulk DOC and HPOA isolates. Ultimately, we aim to strengthen conceptual and empirical linkages between soil C accumulation, freeze-thaw dynamics, and DOM leached from soils to rivers in the northern permafrost region.

2. Methods

2.1. Study Sites

We selected sites within the Beaver, Birch, and Hess Creeks watersheds in interior Alaska to examine DOM radiocarbon abundance and composition in relation to hydrology and permafrost configuration (Table 1).

Table 1. Study Site Locations, Mean Dissolved Organic Carbon (DOC) Concentrations, and Optical Properties of Dissolved Organic Matter (DOM)[a]

Study Site	Latitude[b] (°N)	Longitude[b] (°W)	Watershed Area (km^2)	DOC ($mgC\ L^{-1}$)	a_{254} (m^{-1})	$S_{275-295}$ ($\times 10^{-3}\ nm^{-1}$)
Beaver Creek Watershed						
Above Victoria Creek	65.8056	146.6486	3315	6.1 ± 1.1 (22)	20.5 ± 4.6 (22)	15.10 ± 0.39 (17)
Near Michel Lake	66.2217	146.7621	6164	7.4 ± 1.2 (18)	23.6 ± 5.2 (18)	16.28 ± 0.40 (13)
Birch Creek Watershed						
Above 12 Mile Creek	65.3925	145.7125	231	9.5 ± 7.7 (14)	36.8 ± 8.8 (14)	13.07 (1)
Above Forks	66.2691	145.4953	–	8.1 (1)	28.8 (1)	13.26 (1)
Above Preacher Creek	66.1306	144.8431	–	9.5 (1)	29.4 (1)	15.13 (1)
At Steese Highway Bridge	65.7111	144.3333	5568	16.1 ± 2.5 (28)	61.4 ± 11.5 (28)	12.93 ± 0.22 (3)
Hess Creek Watershed						
At Dalton Highway Bridge	65.6653	149.0964	1715	23.5 ± 1.0 (56)	86.8 ± 4.0 (56)	15.35 ± 1.01 (7)
At confluence with Yukon	65.665	149.7931	3082	19.3 ± 1.4 (11)	68.9 ± 5.6 (11)	14.79 (1)

[a]Plus/minus represents standard error of the mean (SEM). Values in parentheses indicate sample size.
[b]GPS coordinates were recorded using datum NAD83.

All three watersheds are major tributaries of the main-stem of the Yukon River (Figure 1) and are in Alaska's boreal forest region. Discharge data for the creeks were obtained from the U.S. Geological Survey National Water Information System (http://waterdata.usgs.gov/nwis). The Yukon River flows east to west through the discontinuous permafrost zone (50–90% of land area underlain by permafrost), making it an ideal high-latitude watershed to evaluate the impacts of permafrost thaw on riverine C dynamics [*O'Donnell et al.*, 2012a]. The regional climate is strongly continental, with temperature extremes ranging from −50 to 35°C, and annual precipitation averaging 270 mm. Between 1949 and 2013, mean annual air temperature for Fairbanks, Alaska, has increased by 3°C, with the majority of this warming occurring during winter (Alaska Climate Research Center, www.akclimate.org).

The Beaver Creek and Birch Creek watersheds are situated within the Yukon Flats basin, as designated by *Walvoord et al.* [2012]. Beaver Creek above Victoria Creek drains a watershed characterized by mountainous headwaters with exposed bedrock and rubble and a marginal upland area, underlain by ice-rich Pleistocene

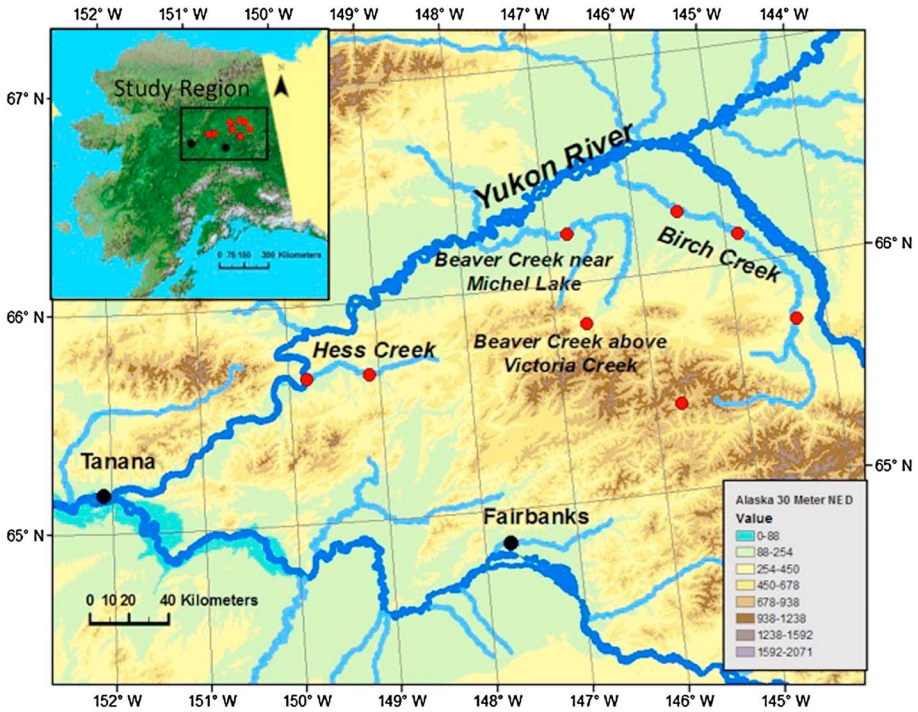

Figure 1. Map of study region. Map inset shows state of Alaska with a black box demarcating the study region. The large map shows the study sites (yellow circles) where samples were collected in the Beaver, Birch, and Hess Creek watersheds in the Yukon River basin. See Table 1 for more detailed site information.

silt, commonly referred to as yedoma [*O'Donnell et al*., 2011a; *Walvoord et al*., 2012]. The Beaver Creek near Michel Lake site is downriver from the Victoria Creek site, and drains an alluvial lowland landscape, characterized by numerous lakes formed on alluvial fans, terraces, and floodplains [*Roach et al*., 2011]. Birch Creek also originates in a mountainous upland region and eventually flows through a portion of the Yukon Flats basin characterized by poorly drained soils and thick peat deposits. Both Beaver and Birch Creeks have been mapped within the discontinuous permafrost region. Permafrost is typically absent under large rivers and lakes, and open taliks (thawed soils) beneath water bodies can allow for hydrologic connectivity between supra- and sub-permafrost aquifers [*Jepsen et al*., 2013; *Wellman et al*., 2013]. Dominant forest vegetation types within these watersheds are primarily black spruce (*Picea mariana*), white spruce (*Picea glauca*), paper birch (*Betula neoalaskana*), quaking aspen (*Populus tremuloides*), and balsam poplar (*Populus balsamifera*).

The Hess Creek watershed is characterized by broad, rounded mountains of the Yukon-Tanana Uplands [*Nowacki et al*., 2001] and deep peat deposits in valley bottoms [*O'Donnell et al*., 2009]. Recent field studies near Hess Creek have reported the presence of yedoma at various hillslope positions [*O'Donnell et al*., 2011a; *Kanevskiy et al*., 2012]. Based on a series of borehole measurements, *Kanevskiy et al*. [2012] report that frozen loess deposits ranged in thickness from 1 to 26 m. Also, segregated ice volume ranged from 60 to 90% by volume, and ice wedges account for between 30 and 50% of permafrost soil volume. While the Hess Creek watershed has been broadly mapped in the discontinuous permafrost zone [*Jorgenson et al*., 2008], permafrost extent is effectively continuous at the local scale across forested hill slopes [*Koch et al*., 2013]. *P. mariana* is the dominant forest type in mature stands at upland and valley bottom topographic positions. Shrubs (e.g., *Salix pulchra*) and *B. neoalaskana* dominate in recently burned stands [*O'Donnell et al*., 2011a].

2.2. DOC Concentration and DOM Chemical Fractionation

Water samples were collected from study sites during spring snowmelt (1 May to 30 June), summer-autumn (1 July 1 to 31 October), and winter (1 November to 30 April) between the years 2002 and 2011 following standard methods [e.g. *Aiken et al*., 2014]. DOC concentrations were determined using an O.I. Analytical Model 700 TOC analyzer via the platinum catalyzed persulfate wet oxidation method [*Aiken et al*., 1992] at the U.S. Geological Survey in Boulder, Colorado. Stream water samples were chromotographically separated into different fractionations: hydrophobic acids (HPOA), hydrophobic neutrals (HPON), hydrophilic organic matter (HPI), and transphilic acids (TPIA) using Amberlite XAD-8 and XAD-4 resins [*Aiken et al*., 1992]. The resins preferentially sorb different classes of organic acids based on aqueous solubility of the solute, chemical composition of the resin, resin surface area, and resin pore size. The amount of organic matter within each fraction, expressed as a percentage of the total DOC concentration, was calculated using the DOC concentration and the sample mass of each fraction. The standard deviation for the mass percentages of the fractionation was ±2%. The HPOA fraction was desalted and lyophilized using the procedure described in *Spencer et al*. [2010] to obtain samples suitable for isotopic analysis.

2.3. DOM Isotopes

We analyzed radiocarbon ($\Delta^{14}C$) content of bulk DOC samples ($\Delta^{14}C$-DOC; $n = 9$) and of the HPOA fraction ($\Delta^{14}C$-HPOA; $n = 33$) to evaluate the age of DOM in relation to seasonal thawing of the active layer and discharge. All samples were sent to the Center for Acceleratory Mass Spectrometry (AMS) at Lawrence Livermore National Laboratory for $\Delta^{14}C$ analysis. Bulk DOC samples were prepared for isotopic analysis following established photo-oxidation methods [*Raymond and Bauer*, 2001; *Butman et al*., 2012]. Subsamples for ^{14}C-DOC analysis were placed in acid-washed 125 mL polycarbonate bottles, acidified to pH 2.5 using 60% phosphoric acid (H_3PO_4), frozen, and shipped to Yale University. At Yale, acidified samples were sparged with ultra-high purity dinitrogen gas (N_2) for 10 min to remove inorganic CO_2. Ultra-high purity oxygen (O_2) was then bubbled through the samples for 5 min followed by sample irradiation for 5 h using a high-energy ultraviolet (UV) light to convert DOC to CO_2. The CO_2 was then trapped and cryogenically purified within the vacuum system using liquid nitrogen, and then sealed in a combusted 6 mm Pyrex tube. In addition to samples, we ran two oxalic acid II (OXII) process standards (low and high concentration) [*Mann*, 1983] to evaluate the impact of this photo-oxidation procedure on $\Delta^{14}C$ values. For HPOA isolates, we also ran a $\Delta^{14}C$-dead process standard (coal) to evaluate the impact of the lyophilization procedure on $\Delta^{14}C$ values.

Solid-phase HPOA isolates and purified CO_2 from whole-water samples were graphitized in preparation for ^{14}C measurement at the Carbon, Water, & Soils Research Lab in Houghton, Michigan. Samples were combusted at 900°C for 6 h with cupric oxide (CuO) and silver (Ag) in sealed quartz test tubes to form CO_2 gas. The CO_2 was then reduced to graphite through heating at 570°C in the presence of hydrogen (H_2) gas and an iron (Fe) catalyst [*Vogel et al*., 1987]. Graphite targets were then analyzed for radiocarbon abundance [*Davis et al*., 1990] and corrected for mass-dependent fractionation using measured $\delta^{13}C$ values for HPOA and DOC samples according to *Stuiver and Polach* [1977].

Errors reported for radiocarbon data reflect only AMS instrumental error and do not capture uncertainty associated with sample isolation techniques (chromatography, lyophilization, and photo oxidation) or environmental variation in DOC composition. Process blanks (coal) indicated that no contamination occurred during the lyophilization procedure. OXII standards which underwent photo-oxidation indicated a variance of Fm ~0.02, or ~20 per mil (‰) $\Delta^{14}C$ or more. $\delta^{13}C$-HPOA was measured at Michigan Tech University's Forest Ecology Stable Isotope Laboratory in Houghton, Michigan, Ion a Costech 4010 Elemental Analyzer and Thermo Finnigan Delta Plus Isotope Ratio Mass Spectrometer. For $\delta^{13}C$ of bulk DOC, we used the mean for all samples collected in rivers of the Yukon River basin (-26.7 ± 1.1, $n = 38$) to correct $\Delta^{14}C$-DOC for mass-based fractionation effects [G. R. Aiken, unpublished data, 2012].

2.4. DOM Optical Properties

We used several approaches for analyzing and reporting the optical properties of chromophoric DOM (CDOM). Decadal UV-Visible absorbance (A) was measured on bulk DOC samples and HPOA fractions before lyophilization at room temperature using a quartz cell with a path length of 1 cm on an Agilent Model 8453 photo-diode array spectrophotometer. The Naperian absorption coefficient at 254 nm (α_{254}) has been shown to serve as a strong predictor for both DOC concentration and $\Delta^{14}C$-DOC in the YRB system [*Spencer et al*., 2009; *O'Donnell et al*., 2012a; *Aiken et al*., 2014]. We determined specific UV absorbance ($SUVA_{254}$) on HPOA isolates by dividing the decadal absorption coefficient at $\lambda = 254$ nm (A_{254}) by DOC concentration, which is common practice [*Aiken*, 2014]. $SUVA_{254}$, which is typically used as an index of DOC aromaticity [*Weishaar et al*., 2003], is reported in units of L mgC m^{-1}. *Weishaar et al*. [2003] also showed that UV absorbance values can be influenced by the presence of iron (Fe). For bulk DOC samples containing Fe, we applied correction factors based on experimental work by *Poulin et al*. [2014], who observed a significant positive correlation between A_{254} and the concentration of Fe^{3+}, reflected by the equation $A_{254\text{-}corrected} = A_{254\text{-}measured} - 0.0687 \times [Fe^{3+}]$ ($R^2 = 0.98$; $P < 0.0001$; $n = 22$). Using this relationship, we corrected A_{254} for samples where we measured total Fe concentration (using the FerroVer Hach spectrophotometric method). Total Fe concentration averaged 0.23 ± 0.04, 0.32 ± 0.11, and 0.94 ± 0.28 mg L^{-1} for samples collected in the Beaver, Birch, and Hess Creek watersheds, respectively.

Spectral slope (S) was calculated by fitting an exponential equation to the absorption spectra between 275 and 295 nm using

$$\alpha_g(\lambda) = \alpha_g(\lambda_{ref}) e^{-S(\lambda - \lambda_{ref})} \quad (1)$$

where $\alpha_g(\lambda)$ is the Naperian absorption coefficient of CDOM at a specified wavelength, λ_{ref} is a reference wavelength, and S is the slope fitting parameter [*Spencer et al*., 2008]. The spectral slope of the 275–295 nm region ($S_{275-295}$) has been shown to be negatively correlated with the molecular weight of DOM [*Helms et al*., 2008]. Prior studies have shown the $S_{275-295}$ to be sensitive to changes in DOM source (e.g., riverine vs. estuarine vs. open ocean) [*Helms et al*., 2008].

Fluorescence excitation-emission matrices (EEMs) were measured on whole-water and HPOA fractions before lyophilization at room temperature using a Jobin-Yvon Horiba Fluoromax-3 fluorometer. Samples were diluted to minimize inner filter effects with deionized water, when necessary, to a decadal UV absorbance at $\lambda = 254$ nm of 0.2 absorbance units (cm^{-1}). EEMs were collected using a 5 nm bandpass for both excitation and emission over an excitation range of 240–450 nm every 5 nm, and an emission range of 300–600 nm every 2 nm in a 1 cm quartz cuvette. Scans were corrected for instrument optics, inner filter corrected, Raman area normalized, Raman normalized blank subtracted, and multiplied by the dilution factor if necessary [*Murphy et al*., 2010]. Resulting EEMs are reported in Raman Units (RU; see supporting information for detailed results). Fluorescence index (FI) was determined as the ratio of the intensities at excitation (ex) and emission

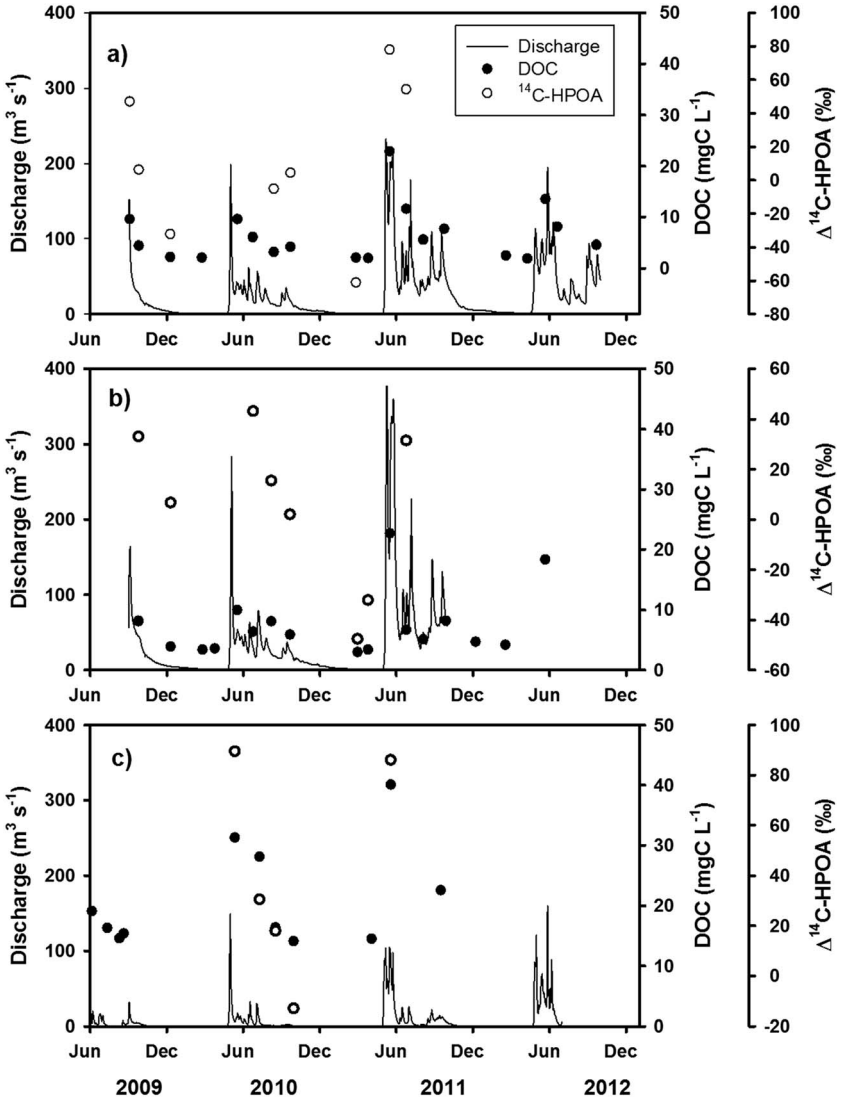

Figure 2. Seasonal variation in river discharge, dissolved organic carbon (DOC) concentration, and Δ^{14}C-HPOA at Beaver Creek above Victoria Creek, (b) Beaver Creek near Michel Lake, and (c) Hess Creek.

Table 2. Summary of DOM Chemical Fractions (% of total DOC) and $SUVA_{254}$ of the Hydrophobic Organic Acid (HPOA) Fraction[a]

Site Name	*n*	HPOA (%)	HPON (%)	TPIA (%)	HPI (%)	HPOA $SUVA_{254}$ (L mgC m^{-1})
Beaver Creek						
Above Victoria Creek	22	48 ± 6	8 ± 4	20 ± 3	19 ± 4	3.2 ± 0.7
Near Michel Lake	18	49 ± 4	8 ± 3	20 ± 2	18 ± 3	3.1 ± 0.6
Birch Creek						
Upper Branch	7	53 ± 4	9 ± 1	18 ± 2	16 ± 2	4.1 ± 0.1
Above 12 Mile Creek	14	55 ± 5	5 ± 3	17 ± 3	17 ± 5	4.1 ± 0.6
Above Forks	1	53	8	20	16	2.9
Above Preacher Creek	1	52	9	20	17	2.9
At Steese Highway Bridge	28	53 ± 3	8 ± 3	17 ± 2	16 ± 2	3.8 ± 0.6
Hess Creek						
At Dalton Highway Bridge	59	54 ± 3	6 ± 2	19 ± 2	15 ± 2	3.9 ± 0.4
At Mouth	11	54 ± 2	6 ± 4	19 ± 1	15 ± 1	3.7 ± 0.3

[a]Plus/minus represents standard error of the mean (SEM). HPOA = hydrophobic organic acids, HPON = hydrophobic neutrals, TPIA = transphilic organic acids, and HPI = low molecular-weight hydrophilic compounds.

Table 3. Summary of Stable Isotope and Radiocarbon Data for Three Study Watersheds

Sample Date	Site Name	Sample Type	$\delta^{13}C$ (‰)	Fraction Modern	$\Delta^{14}C$ (‰)	^{14}C Age (yr BP)
Beaver Creek Watershed						
6/24/2011	Above Victoria Creek	Bulk DOC	−26.7	1.043 ± 0.004	35.2 ± 3.7	Modern
8/12/2009	Above Victoria Creek	HPOA isolate	−27.7	1.002 ± 0.003	−5.1 ± 2.5	Modern
9/3/2009	Above Victoria Creek	HPOA isolate	−27.9	1.055 ± 0.003	47.1 ± 3.1	Modern
9/21/2009	Above Victoria Creek	HPOA isolate	−27.8	1.012 ± 0.003	4.5 ± 3.0	Modern
9/24/2009	Above Victoria Creek	HPOA isolate	−27.8	1.014 ± 0.003	6.4 ± 2.7	Modern
12/8/2009	Above Victoria Creek	HPOA isolate	−27.7	0.975 ± 0.003	−32.2 ± 2.7	205 ± 25
2/22/2010	Above Victoria Creek	HPOA isolate	−27.6	1.001 ± 0.003	−6.6 ± 3.2	0 ± 30
2/24/2011	Above Victoria Creek	HPOA isolate	−27.3	0.946 ± 0.003	−61.0 ± 2.8	445 ± 25
5/16/2011	Above Victoria Creek	HPOA isolate	−28.2	1.086 ± 0.003	77.9 ± 2.9	Modern
6/24/2011	Above Victoria Creek	HPOA isolate	−28.1	1.062 ± 0.005	54.4 ± 4.9	Modern
2/28/2011	Near Michel Lake	Bulk DOC	−26.7	0.954 ± 0.003	−52.7 ± 3.4	375 ± 30
6/24/2011	Near Michel Lake	Bulk DOC	−26.7	1.019 ± 0.004	11.7 ± 3.6	Modern
12/9/2009	Near Michel Lake	HPOA isolate	−27.7	1.014 ± 0.003	6.7 ± 2.9	Modern
6/24/2010	Near Michel Lake	HPOA isolate	−27.9	1.051 ± 0.004	43.3 ± 3.8	Modern
8/6/2010	Near Michel Lake	HPOA isolate	−27.7	1.023 ± 0.004	15.5 ± 4.2	Modern
9/20/2010	Near Michel Lake	HPOA isolate	−27.7	1.010 ± 0.003	2.1 ± 3.3	Modern
2/28/2011	Near Michel Lake	HPOA isolate	−27.5	0.960 ± 0.004	−47.6 ± 3.9	330 ± 35
3/25/2011	Near Michel Lake	HPOA isolate	−27.5	0.975 ± 0.003	−32.1 ± 2.8	205 ± 25
6/24/2011	Near Michel Lake	HPOA isolate	−27.9	1.039 ± 0.003	31.5 ± 3.4	Modern
Birch Creek Watershed						
3/21/2011	Above Preacher Creek	Bulk DOC	−26.7	0.971 ± 0.004	−36.4 ± 3.5	240 ± 30
5/27/2011	Above 12 Mile Creek	Bulk DOC	−26.7	1.104 ± 0.004	96.1 ± 3.9	Modern
5/27/2011	At Steese Highway Bridge	Bulk DOC	−26.7	1.086 ± 0.004	78.0 ± 3.9	Modern
4/2/2002	At Steese Highway Bridge	HPOA isolate	−28	1.091 ± 0.003	83.3 ± 3.1	Modern
6/8/2002	Above 12 Mile Creek	HPOA isolate	−27.8	1.099 ± 0.003	90.5 ± 3.1	Modern
6/21/2002	Upper Birch Creek	HPOA isolate	−27.9	1.110 ± 0.004	102.2 ± 3.5	Modern
8/31/2002	Upper Birch Creek	HPOA isolate	−27.8	1.077 ± 0.003	68.9 ± 3.4	Modern
3/29/2003	At Steese Highway Bridge	HPOA isolate	−27.4	0.985 ± 0.003	−22.1 ± 2.8	120 ± 25
3/21/2011	Above Preacher Creek	HPOA isolate	−27.8	0.987 ± 0.003	−20.2 ± 3.4	105 ± 30
3/23/2011	Above Forks	HPOA isolate	−27.7	0.987 ± 0.003	−19.9 ± 2.8	100 ± 25
5/27/2011	Above 12 Mile Creek	HPOA isolate	−28.1	1.110 ± 0.003	101.8 ± 3.2	Modern
5/27/2011	At Steese Highway Bridge	HPOA isolate	−28.1	1.079 ± 0.003	70.6 ± 3.1	Modern
Hess Creek Watershed						
7/9/2010	At Dalton Highway Bridge	Bulk DOC	−26.7	1.062 ± 0.004	54.4 ± 4.3	Modern
9/29/2010	At Dalton Highway Bridge	Bulk DOC	−26.7	0.988 ± 0.004	−19.1 ± 3.5	95 ± 30
5/18/2011	At Dalton Highway Bridge	Bulk DOC	−26.7	1.102 ± 0.004	93.9 ± 3.9	Modern
4/1/2002	At Dalton Highway Bridge	HPOA isolate	−27.7	1.014 ± 0.003	33.6 ± 2.7	Modern
3/28/2008	At Dalton Highway Bridge	HPOA isolate	−27.6	0.996 ± 0.003	−11.4 ± 2.9	35 ± 25
8/28/2008	At Yukon River confluence	HPOA isolate	−27.7	1.017 ± 0.005	9.2 ± 4.8	Modern
5/11/2010	At Dalton Highway Bridge	HPOA isolate	−28.1	1.098 ± 0.004	89.5 ± 4.0	Modern
7/9/2010	At Dalton Highway Bridge	HPOA isolate	−28	1.038 ± 0.004	30.5 ± 3.5	Modern
8/16/2010	At Dalton Highway Bridge	HPOA isolate	−27.8	1.026 ± 0.003	18.0 ± 2.7	Modern
9/29/2010	At Dalton Highway Bridge	HPOA isolate	−27.4	0.994 ± 0.004	−12.9 ± 4.0	45 ± 35
5/18/2011	At Dalton Highway Bridge	HPOA isolate	−28.2	1.094 ± 0.004	86.1 ± 3.7	Modern

(em) wavelengths ex370/em470 and ex370/em520 [*Cory et al.*, 2010]. We used linear and nonlinear regression techniques to evaluate relationships between $\Delta^{14}C$-HPOA and various measures of CDOM composition (a_{254}, $SUVA_{254}$, $S_{275-295}$, FI).

3. Results

3.1. Spatial and Temporal Patterns of DOM Concentration and Composition

DOC concentration at our study sites varied both over space (Table 1) and time (Figure 2a). Mean DOC concentration was generally greater at sites in the Hess Creek watershed, relative to sites in the Beaver and Birch Creek watersheds. In all watersheds DOC concentration was greatest during spring snowmelt, averaging $12.4 \pm 1.9\,mgC\,L^{-1}$ in the Beaver Creek watershed sites, $17.2 \pm 3.2\,mgC\,L^{-1}$ at the Birch Creek sites, and

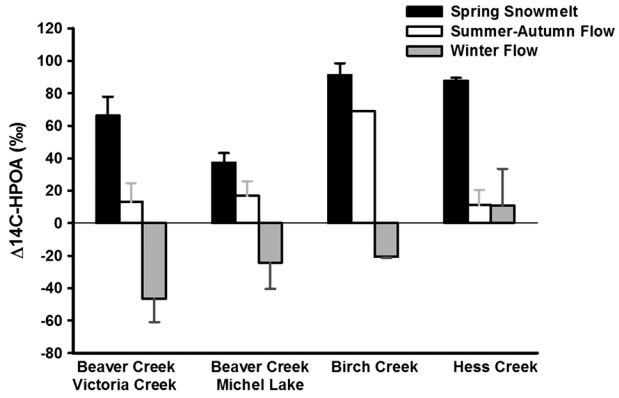

Figure 3. Mean $\Delta^{14}C$ of the hydrophobic organic acid (HPOA) fraction (‰; ±one standard error of the mean (SEM)) across seasons and study sites. Here, Birch and Hess Creek values reflect samples collected from all sites within the watershed.

28.2 ± 1.2 mgC L^{-1} in Hess Creek. DOC concentrations were lowest during winter flow, averaging 2.9 ± 0.2 mgC L^{-1} at the Beaver Creek sites, 6.1 ± 0.6 mgC L^{-1} at the Birch Creek sites, and 15.5 ± 0.5 mgC L^{-1} in Hess Creek. Temporal variation in DOC concentrations was strongly linked to seasonal changes in discharge at the Beaver Creek study sites (Figures 2a and 2b) and at Hess Creek (Figure 2c). We observed the greatest DOC concentrations during peak discharge events during spring snowmelt and the lowest DOC concentrations during winter flow. DOC concentrations during summer and autumn were variable, but appeared to correlate positively to summer storm events.

HPOA was the dominant DOM fraction observed at our study sites, averaging 52 ± 5% across all sites and seasons (Table 2). HPI and TPIA composed a smaller proportion of the DOM pool, averaging 17 ± 3 and 19 ± 3%, respectively. We observed considerable variability in DOM fractions across seasons. For instance, the HPOA fraction varied significantly across seasons (ANOVA, df = 2, $F = 18.26$, $P < 0.001$), and was greatest during spring snowmelt (mean = 55 ± 4% for all study sites combined) and lowest during winter flow (49 ± 5%). The HPI fraction also varied significantly across seasons (df = 2, $F = 27.61$, $P < 0.001$), and was lowest during spring snowmelt (15 ± 2%) and greatest during winter flow (19 ± 4%). Mean $SUVA_{254}$ of the HPOA fraction for all sites combined was 3.6 ± 0.7 L mgC m^{-1}, with highest values observed during spring snowmelt (4.2 ± 0.3 L mgC m^{-1}) and lowest values during winter flow (2.8 ± 0.5 L mgC m^{-1}).

Mean α_{254} values were greatest at Hess Creek (Dalton Highway), averaging 86.8 ± 4.0 m^{-1}, and lowest at Beaver Creek above Victoria Creek, averaging 20.5 ± 4.6 m^{-1} (Table 1). $S_{275-295}$ averaged 15.26 ± 1.83 × 10^{-3} nm^{-1} across all study sites and seasons (Table 1), which is within the mean range of samples reported for 30 watersheds in the contiguous United States (13.00–16.50 × 10^{-3} nm^{-1}) [*Spencer et al.*, 2012]. The shallowest spectral slopes, which are associated with high molecular weight and aromatic DOM, were observed during spring snowmelt, whereas the steepest spectral slopes were observed during winter flow. Mean FI values ranged from 1.37 to 1.45 across study sites, reflecting a mixture of terrestrial- and microbially derived CDOM [*McKnight et al.*, 2001].

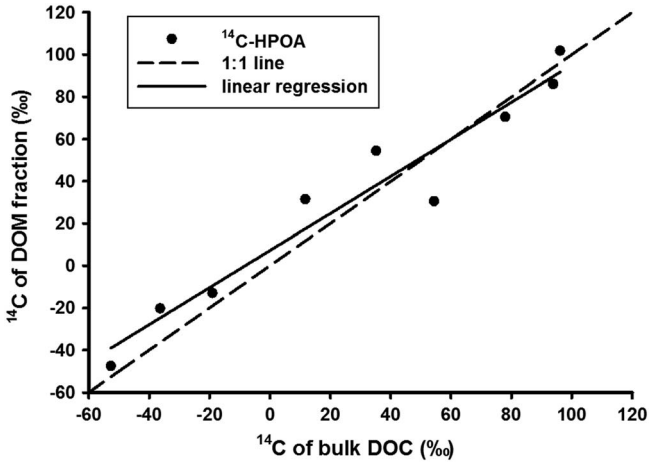

Figure 4. Relationship between $\Delta^{14}C$ of HPOA and $\Delta^{14}C$ of bulk DOC on a subset of stream water samples. The dashed line is the 1:1 line, while the solid line represents a regression line fit to the data and described by the equation $y = 0.88x + 7.21$ ($R^2 = 0.94$, $P < 0.0001$).

3.2. Spatial and Temporal Patterns in $\Delta^{14}C$ of DOM

We observed strong seasonal controls on $\Delta^{14}C$-HPOA across study sites (Table 3 and Figure 3). In general, $\Delta^{14}C$-HPOA values were greatest during spring snowmelt (mean $\Delta^{14}C = 73.0 \pm 8.4$‰ for all sites), reflecting the dominance of modern C during this period. During winter flow, $\Delta^{14}C$-HPOA values were generally lower relative to spring snowmelt and summer-autumn flow; however, we observed differences in $\Delta^{14}C$-HPOA values of winter flow across sites (Figure 3). For the Beaver and Birch Creek study sites, mean

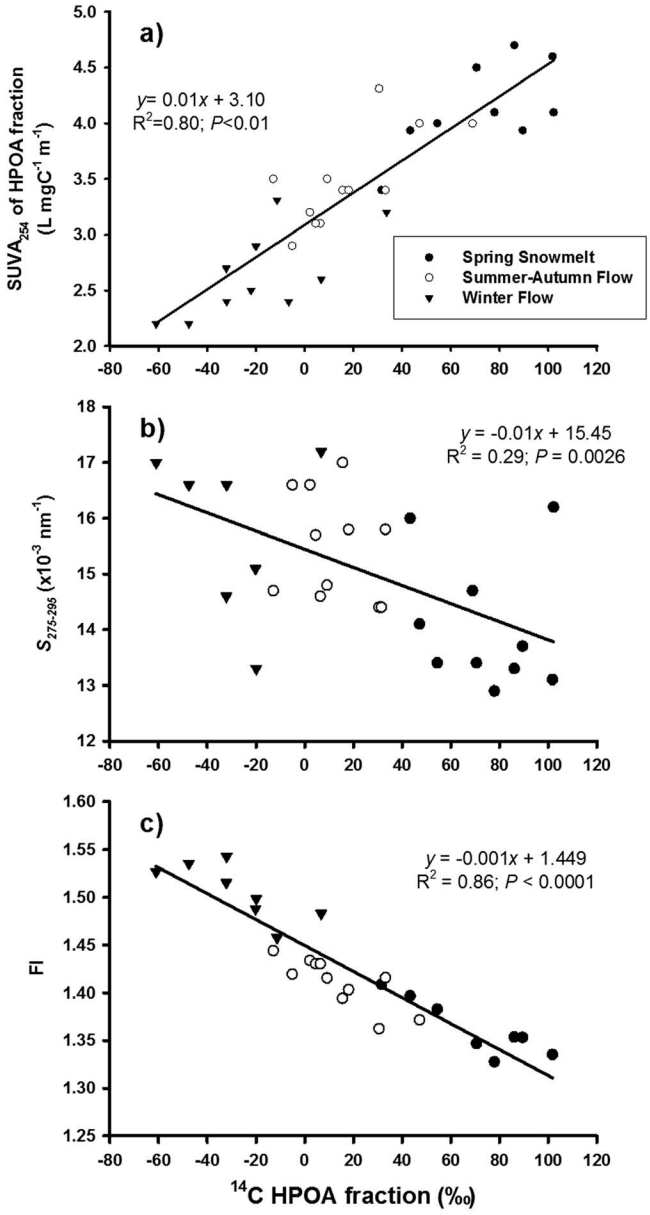

Figure 5. Linear relationship between (a) $SUVA_{254}$ of the HPOA fraction, (b) $S_{275–295}$ of the bulk DOC, and (c) and fluorescence index (FI) of the bulk DOC and Δ^{14}C-HPOA across seasons. For our analyses, spring snowmelt is defined as 1 May to 30 June, summer-autumn flow as 1 July to 30 September, and winter flow as 1 October to 30 April.

Δ^{14}C-HPOA values were negative, indicating the flux of older C during winter flow (Figure 3). Radiocarbon age of HPOA during winter flow for these study sites ranged from 100 to 445 yr BP (Table 3). At Hess Creek, mean Δ^{14}C-HPOA values during winter flow were positive, and of similar magnitude to samples collected during summer-autumn flow. Δ^{14}C-HPOA values at the Beaver and Hess Creek study sites were correlated to mean daily discharge (Supplemental Table 2). On a subset of water samples, we also measured the Δ^{14}C of bulk DOC (Δ^{14}C-DOC) to evaluate the relationship with Δ^{14}C-HPOA measurements and thus its broader utility as an indicator of DOC age. Δ^{14}C-HPOA was positively and significantly correlated with Δ^{14}C-DOC across different sites and sampling times ($R^2 = 0.94$, $P < 0.0001$; Figure 4).

3.3. Relationship Between Δ^{14}C of DOM and DOM Composition

We observed a positive linear relationship between $SUVA_{254}$ of the HPOA fraction and Δ^{14}C-HPOA for all sites combined ($R^2 = 0.80$, $P < 0.01$; Figure 5a). Our findings revealed a strong seasonal pattern to this relationship: during spring snowmelt, DOM was composed of highly aromatic modern C, whereas during winter flow, DOM was ^{14}C-depleted and less aromatic. We also observed a negative linear relationship between $S_{275–295}$ and Δ^{14}C-HPOA ($R^2 = 0.29$, $P = 0.0026$; Figure 5b). This pattern indicates that during spring snowmelt, ^{14}C-enriched DOM has higher molecular weight (i.e., shallower spectral slope) relative to the ^{14}C-depleted DOM during winter flow. FI was also negatively correlated with Δ^{14}C-HPOA ($R^2 = 0.86$, $P < 0.0001$; Figure 5c). During spring snowmelt, ^{14}C-enriched DOM was primarily of terrestrial origin, whereas ^{14}C-depleted DOM during winter flow was a mixture of terrestrial-derived and microbially derived organic matter. We acknowledge that autocorrelation, if present, would weaken the apparent relationship between DOM composition variables and Δ^{14}C-HPOA.

HPOA concentration and Δ^{14}C-HPOA were both significantly correlated with α_{254} values of bulk DOC samples (Figure 6a). Nearly 98% of the variation in HPOA concentration is explained by a linear relationship with α_{254} ($P < .0001$). We observed a positive non-linear relationship between Δ^{14}C-HPOA and α_{254} ($R^2 = 0.50$, $P < 0.0003$). Using this relationship, we examined long-term changes in α_{254} values (as an indicator for DOM

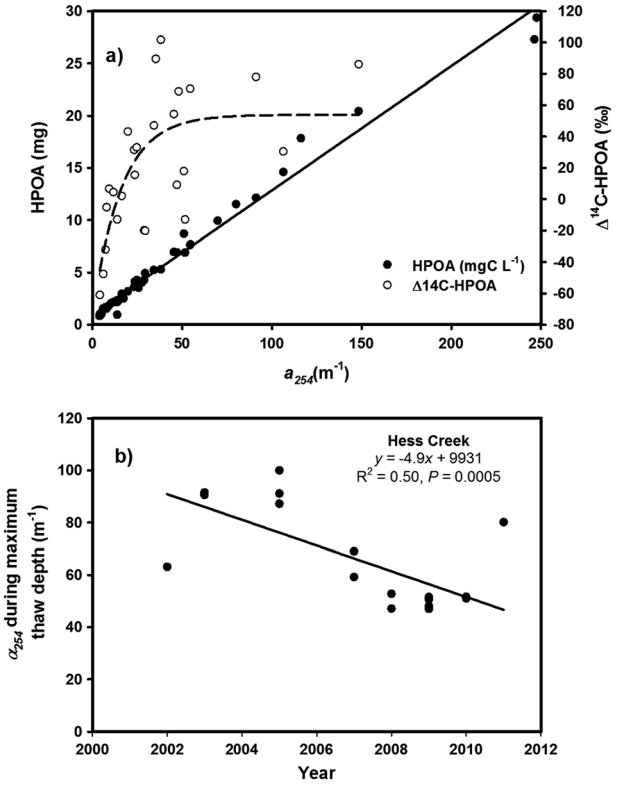

Figure 6. (a) The linear relationship between HPOA concentration and α_{254} from bulk DOC samples is described by the equation $y = 0.12x + 0.95$ ($R^2 = 0.98$, $P < 0.0001$). The nonlinear relationship between Δ^{14}C-HPOA and α_{254} is described by the equation $y = -74 + 128\ (1 - e^{-0.06x})$ ($R^2 = 0.50$, $P = 0.0003$), and closely resembles the relationship between Δ^{14}C-DOC and α_{254} observed by *Aiken et al.* [2014]. (b) Long-term trend in mean α_{254} during maximum thaw depth (August through October) for Hess Creek.

age) of all bulk DOC samples collected during August through October (the period of maximum thaw depth; Figures 7b–7d). At Hess Creek (the only site with a long-term record), we observed a significant negative relationship between α_{254} during maximum thaw depth between 2002 and 2012 ($R^2 = 0.50$, $P = 0.0005$; Figure 6b).

4. Discussion

4.1. Spatial and Temporal Patterns in Δ^{14}C of DOM in Boreal Rivers

At high latitudes, DOM age and composition vary across space and time, as governed by seasonal shifts in flow path and source water contribution to stream discharge [*O'Donnell et al.*, 2010, *O'Donnell et al.*, 2012a]. Here, we observed strong seasonal controls on DOM age, characterized by modern DOM during spring snowmelt, relatively ^{14}C-depleted DOM during winter flow, and DOM of intermediate ^{14}C abundance during summer-autumn flow. Seasonal shifts in DOM age were closely coupled to source water changes as manifested in river discharge (Figure 2), a finding consistent with prior studies in both high-latitude [*Neff et al.*, 2006; *Raymond et al.*, 2007] and temperate regions [*Butman et al.*, 2012]. In arctic and subarctic regions, snowmelt is a major annual hydrologic event, both as a component of annual discharge and in terms of DOC flux [*Finlay et al.*, 2006; *Striegl et al.*, 2007]. During this period, lateral flow from watershed soils is confined to surface runoff and shallow moss and litter layers. The composition of DOM leached from these layers reflects recently fixed soil C that has undergone minimal processing by soil microbes or stabilization by mineral soils, as supported by the enriched Δ^{14}C and high $SUVA_{254}$ values of samples collected during spring snowmelt. Prior work [*Neff et al.*, 2006; *Spencer et al.*, 2008] also reported that during spring snowmelt, DOM from arctic and subarctic rivers is largely composed of undecomposed terrestrial lignin and other aromatic C. In general, winter flow in high-latitude regions is supported by deeper groundwater sources, reflected by the distinctive composition of DOM during this period [*O'Donnell et al.*, 2012a]. For instance, DOM composition during winter flow generally is less aromatic (i.e., lower $SUVA_{254}$ values) and has a higher fraction of low molecular-weight hydrophilic compounds relative to spring snowmelt and summer-autumn flow.

In the Beaver and Birch Creek watersheds, we observed relatively old DOM (Δ^{14}C-HPOA $<$0‰) during winter flow, with DOM age ranging from 100 to 445 yr BP. These values are comparable to other observations within the YRB [*Striegl et al.*, 2007] and other major arctic rivers [*Raymond et al.*, 2007]. Interestingly, radiocarbon age of DOM in this study closely approximates simulated base flow travel times (i.e., travel path of water from point of recharge until it discharges to a stream) under present-day permafrost configurations for Yukon Flats (114 to 335 years), as reported by *Walvoord et al.* [2012]. Together, these observations point toward a more pronounced contribution of older organic matter to these streams and rivers under low flow conditions (e.g., winter flow). By modeling groundwater dynamics across an assumed permafrost thaw sequence, *Walvoord et al.* [2012] also showed that base flow travel times generally increase with thaw in discontinuous

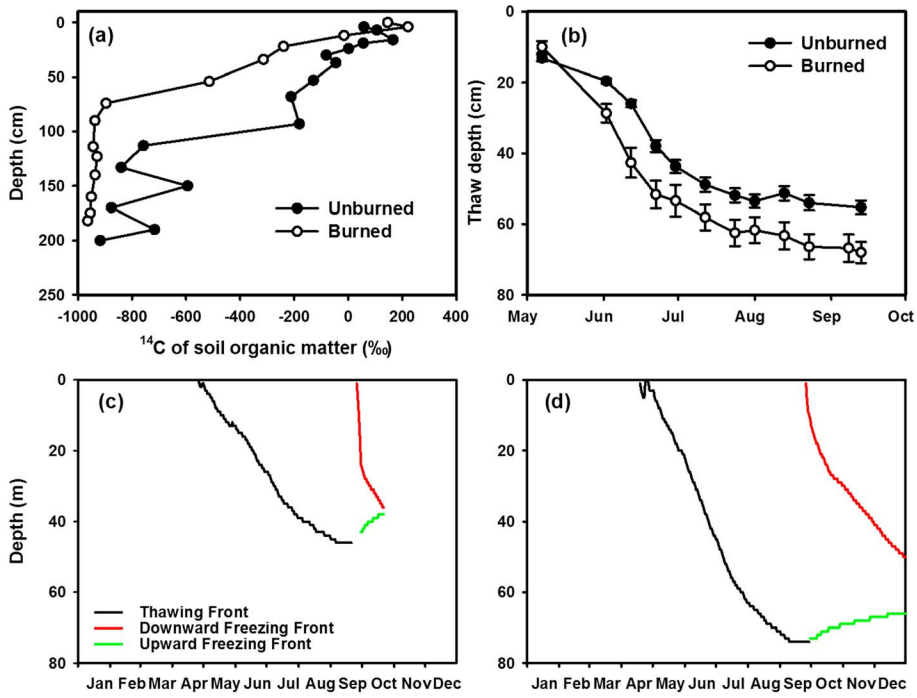

Figure 7. (a) Variation in Δ^{14}C of soil organic matter with soil depth at a burned and unburned stand in the Hess Creek watershed (data from *O'Donnell et al*. [2011a]). (b) Seasonal change in thaw depth at a burned and unburned black spruce stand in the Hess Creek watershed (data from *O'Donnell et al*. [2009]). Freezing and thaw fronts are also plotted for (c) an unburned black spruce stand and (d) a 4 year old burn in the Hess Creek watershed. Freezing and thawing fronts reflect results of site-based simulations using the Geophysical Institute Permafrost Laboratory (GIPL) model (results are modified and re-plotted from *O'Donnell et al*. [2011b]), and highlight the role of fire in governing the vertical extent and duration of deep unfrozen layers.

permafrost. Thus, the apparent correlation between travel times and DOM age provides additional support for the use of DOM as a tool for tracking thaw.

The Hess Creek watershed is underlain by deep yedoma deposits [*O'Donnell et al*., 2011a], and most likely reflects a "continuous" permafrost configuration [*Koch et al*., 2013], where groundwater flows predominantly through the supra-permafrost aquifer and travel times are relatively short [*Walvoord et al*., 2012]. On average, Δ^{14}C-HPOA during winter flow in Hess Creek was not depleted, suggesting that discharge from deep sub-permafrost aquifers is limited. Similar findings have been reported for the Lena River basin in Siberia [*Raymond et al*., 2007]. Using fluorescence spectroscopy, *O'Donnell et al*. [2012a] observed similar CDOM characteristics for samples collected during summer-autumn and winter flow at Hess Creek. We hypothesize that flow in Hess Creek is generated primarily by groundwater discharge from the supra-permafrost aquifer across seasons. Winter flow likely originates from closed taliks (i.e., perennially unfrozen soil layers above the permafrost table) in valley bottoms, where peat deposits exceed 2 m depth [*O'Donnell et al*., 2009]

4.2. Linking DOM Δ^{14}C in Rivers With Soil Thermal Dynamics and Flow Paths in Permafrost Regions

To use DOM age and composition for detecting permafrost thaw, a strong linkage must be established between soil C dynamics, soil thermal dynamics, and DOM leached from soils to surface waters. Vertical patterns in soil C stocks and SOM age provide an initial constraint on potential DOM flux from soils. In the boreal region, a number of studies have measured Δ^{14}C of SOM as a function of depth through soil profiles [*Trumbore and Harden*, 1997; *O'Donnell et al*., 2011; *Hicks Pries et al*., 2012]. In the Hess Creek watershed, *O'Donnell et al*. [2011a] observed a distinct vertical pattern in Δ^{14}C of SOM, with bomb-spike C (positive Δ^{14}C values) incorporated into shallow organic layers and a steady decline in Δ^{14}C with depth through mineral soils of the active layer and near-surface permafrost (Figure 7a). Seasonal thawing of the active layer (Figure 7b) governs both (1) the proportion of soil C in a frozen or unfrozen state [*O'Donnell et al*., 2011a, 2011b], and (2) the depth of subsurface flow paths through active layer soils. Under present-day climate

conditions in these ecosystems, ALT (or maximum annual thaw depth) ranges between 50 and 75 cm (Figures 7b–7d). Interactions between soil thermal and hydrologic dynamics in active layer soils and near-surface permafrost govern the age and amount of SOM subject to leaching and thus control the age and composition of DOM transported laterally from soils to streams.

In addition to climate variability, wildfire can have a profound effect on ALT in the boreal region (Figures 7b–7d) [*Yoshikawa et al*., 2003; *O'Donnell et al*., 2011a, 2011b]. By tracking thawing and freezing fronts using a soil thermal model (Figures 7c and 7d), we can quantify the vertical extent and duration of soils in the frozen and unfrozen state. In an unburned stand, deep soils (between 40 and 50 cm) persist in an unfrozen state through August and September, prior to upward freezing from the permafrost table and downward freezing from the ground surface (Figure 7c). In a recently burned stand, increases in ALT cause even deeper soils (60–75 cm) to persist in an unfrozen state from August through October. Thus, to detect permafrost thaw through changes in ALT, we must focus on DOM leached from these deep unfrozen soil layers in late-summer and autumn. In a companion study, we characterized DOM leached from different boreal soils and showed that DOM yield and aromaticity vary as a function of depth [*O'Donnell et al*., 2012b]. In the present study, we show that DOM age and composition vary seasonally, presumably as depth of subsurface flows change with soil thermal and hydrologic dynamics. To further advance our understanding of the link between DOM in soils and rivers, more work is needed to track DOM transformations along subsurface flow paths of varying complexity and depth in permafrost regions.

4.3. Using Optical Measurements for Detecting Trends in DOM Δ^{14}C and Permafrost Thaw

While Δ^{14}C measurements are a useful tool for determining the age and source of terrestrial DOM in high-latitude rivers, high-frequency monitoring of Δ^{14}C of DOM may be prohibitive given the high analytical cost and complexity of sample extraction and measurement. However, development of optical measurements as indicators of DOM age and composition may provide an inexpensive and simple means for tracking changes in northern rivers. Recent advances in in situ monitoring using optical sensors have allowed for improved flux estimates of DOC [*Spencer et al*., 2009] and nitrogen [*Pellerin et al*., 2011]. Furthermore, the development of optical proxies has improved our understanding of DOM dynamics, including temporal and spatial variations in DOM size class [*Helms et al*., 2008], HPOA percentage [*Spencer et al*., 2012], and lignin phenol composition [*Spencer et al*., 2008]. In the present study, we used a suite of optical measurements to establish relationships with Δ^{14}C of DOM. For instance, we observed a strong positive relationship between aromaticity and age within the HPOA fraction (Figure 5a), indicating that young DOM is highly aromatic and older DOM is more aliphatic, and thus more processed. *Butman et al*. [2012] observed a similar relationship between Δ^{14}C and $SUVA_{254}$ in the bulk DOC pool for rivers in the conterminous United States. We also showed that young DOM generally consists of higher molecular-weight compounds than older DOM in these river systems, as evidenced by the negative correlation between Δ^{14}C and spectral slope ($S_{275-295}$; Figure 5b).

Recent work by *Aiken et al*. [2014] documented a highly significant, nonlinear relationship between Δ^{14}C-DOC and α_{254} in the Yukon River basin, highlighting the potential use of absorbance measurements to track DOM age in high-latitude rivers. Our results further support these findings, as we observed a strong correlation between Δ^{14}C-HPOA and α_{254} (Figure 6a). In each study, Δ^{14}C-DOC and Δ^{14}C-HPOA rise to maximum values (described by the asymptote within the exponential equation) associated with recently fixed bomb-spike ^{14}C. Moreover, we document a highly significant relationship between Δ^{14}C-HPOA and Δ^{14}C-DOC (Figure 4), suggesting that the age of bulk DOC and the HPOA fraction are tightly coupled in these systems. Overall, these observations highlight the utility and importance of archived HPOA isolates as a useful tool for approximating the age of DOC in aquatic systems.

Permafrost thaw in high-latitude systems promotes deeper subsurface flow paths and should result in the release of older DOM (and higher α_{254} values) via (1) increasing ALT and expansion of the supra-permafrost aquifer, or (2) re-enhanced groundwater flow through sub-permafrost aquifers that discharge to streams and rivers [*Bense et al*., 2009; *Walvoord et al*., 2012]. Thermokarst and riverbank erosion has been associated with the release of old POC [e.g., *Guo et al*., 2007], and it is likely that old DOM could also be released through these processes, but difficult to detect in mid- to high-order streams [*Vonk et al*., 2013]. In general, detection of active layer thickening using DOM should be most pronounced during late summer and autumn, when thaw depth reaches an annual maximum. To determine the possible effects of permafrost thaw on DOM age, we examined

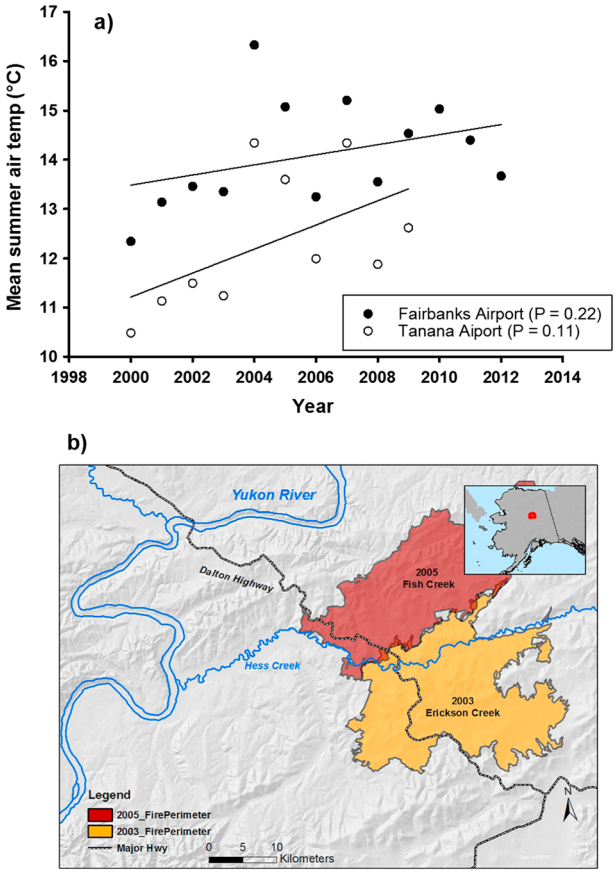

Figure 8. (a) Mean summer air temperature trends for Fairbanks and Tanana for years 2000 through 2012. (b) Map showing two fire perimeters within the Hess Creek watershed.

long-term trends in α_{254} during maximum annual thaw (August through October) at the Hess Creek watershed. We observed a significant negative trend in α_{254} between 2002 and 2012 (Figure 6b), indicating a shift towards older DOM in the last decade. We hypothesize that this shift in DOM age is primarily due to watershed-scale deepening of subsurface flow paths as a consequence of both wildfire and permafrost thaw. Hess Creek is a low gradient, blackwater river [*O'Donnell et al.*, 2010] that drains a forest watershed underlain by thick, ice-rich yedoma deposits [*O'Donnell et al.*, 2011a; *Kanevskiy et al.*, 2012]. As a result, flow in Hess Creek is generated primarily via inputs from the supra-permafrost aquifer, and DOM input from sub-permafrost aquifers is negligible [*O'Donnell et al.*, 2012a]. During this period (2002–2012), air temperatures near Hess Creek warmed marginally (Figure 8a), and two significant wildfires burned within the Hess Creek catchment (Figure 8b). The combined effects of climate and wildfire can have a profound effect on permafrost, accelerating rates of thaw through increases in ALT [*O'Donnell et al.*, 2011b] and thermokarst [*Osterkamp et al.*, 2000].

Despite this decreasing trend in α_{254} (and in turn, $\Delta^{14}C$), it appears that riverine DOM is of modern origin (where $\alpha_{254} > 20\,m^{-1}$ and $\Delta^{14}C$-HPOA $>0‰$; Figure 6b) and not from thawed permafrost. We hypothesize that permafrost thaw through increasing ALT has allowed for decomposition of soil organic matter that has accumulated in mineral soils during the Holocene (see Figure 7). Post-thaw release of Holocene-aged DOM may have occurred but was not detected in the river. Recent work by *Vonk et al.* [2013] documents that DOM released from yedoma is highly labile and susceptible to rapid mineralization. In a companion study [*Ewing et al.*, in review], we documented the presence of ancient DOM from the late-Pleistocene in yedoma deposits in the Hess Creek watershed. At present, deeper Pleistocene-age deposits within the basin appear to be relatively resilient to recent warming and disturbance from wildfire [*O'Donnell et al.*, 2011a; *Kanevskiy et al.*, 2012; *Jorgenson et al.*, 2013] due to the high latent-heat content of these ice-rich yedoma deposits [*Romanovsky et al.*, 2010]. However, projected warming and changes to the wildfire regime may promote permafrost thaw [*O'Donnell et al.*, 2011b] and the subsequent release of DOM from these yedoma deposits. Our observations suggest that the application of absorbance measurements as indicators for $\Delta^{14}C$ of DOM may serve as a promising tool for detecting permafrost thaw and associated changes to watershed hydrology.

5. Conclusions

DOM composition is a powerful tool for evaluating watershed processes associated with changing climate, land use change, and other disturbances. Recent studies have highlighted the sensitivity of DOM composition to watershed permafrost configuration [*O'Donnell et al.*, 2012a]; in turn, DOM may serve as a useful tool for detecting thaw within a basin. Using optical properties of CDOM in high-latitude rivers to identify permafrost thaw may have some unique advantages over traditional monitoring approaches. While permafrost thaw has been detected through monitoring of borehole temperatures and ALT [e.g., *Romanovsky et al.*, 2010], these measurements have limited spatial inference and primarily reflect local conditions. Remote sensing analyses

have also been useful for detecting thermokarst features [e.g., *Jorgenson et al.*, 2006], yet have limited application in upland forests or in ice-poor regions not susceptible to ground subsidence. Analysis of stream discharge time-series (e.g., recession flow analysis) can be a powerful tool for identifying watershed-scale changes in ALT [e.g., *Lyon and Destouni*, 2010], but long-term hydrologic data are sparse in many northern regions. CDOM measurements (e.g., α_{254}) are presently tightly linked to DOM age and composition, and thus serve as inexpensive indicators for radiocarbon measurements at this time. This technique for detecting thaw may prove useful to long-term aquatic monitoring programs in the Arctic, where access to remote sites is often prohibitive by cost and logistics. Future research should aim to improve our understanding of the linkages between permafrost architecture, its vulnerability to thaw, and post-thaw controls on DOM transport and composition.

Acknowledgments

Funding for this project was provided by the National Research Program and Climate Effects Network of the Water, Climate, and Land Use Change Mission Areas of the US Geological Survey. The manuscript was greatly improved thanks to comments by the Editor, Associate Editor, two anonymous reviewers, and Brett Poulin. We would like to thank Karena Schmidt (Michigan Tech) for graphitizing HPOA isolates and Jennifer Eikenberry (Michigan Tech) for analyzing ^{13}C content of HPOA isolates. We also thank Heather Best (USGS Fairbanks) for helping with field logistics and sample collection and Jennifer Barnes for assistance in making Figure 8b. Interested users can contact the corresponding author for access to data presented and analyzed here. Any use of trade, firm, or product names is for descriptive purposes only and does not imply endorsement by the U.S. Government.

References

Aiken, G. R. (2014), Fluorescence and dissolved organic matter: A chemist's perspective, in *Aquatic Organic Matter Fluorescence*, pp. 35–74, Cambridge Univ. Press, Cambridge, U. K.

Aiken, G. R., D. M. McKnight, K. A. Thorn, and E. M. Thurman (1992), Isolation of hydrophilic organic acids from water using nonionic macroporous resins, *Org. Geochem.*, *4*, 567–573.

Aiken, G. R., R. G. M. Spencer, R. G. Striegl, P. F. Schuster, and P. A. Raymond (2014), Influences of glacial melt and permafrost thaw on the age of dissolved organic carbon in the Yukon River basin, *Global Biogeochem. Cycles*, *28*, 525–537, doi:10.1002/2013GB004764.

Aufdenkampe, A. K., E. Mayorga, P. A. Raymond, J. M. Melack, S. C. Doney, S. R. Alin, R. E. Aalto, and K. Yoo (2011), Riverine coupling of biogeochemical cycles between land, oceans, and atmosphere, *Front. Ecol. Environ.*, *9*, 53–60, doi:10.1890/100014.

Balcarczyk, K. L., J. B. Jones, R. Jaffe, and N. Maie (2009), Stream dissolved organic matter bioavailability and composition in watersheds underlain by discontinuous permafrost, *Biogeochemistry*, *94*, 255–270, doi:10.1007/s10533-009-9324-x.

Benner, R., B. Benitez-Nelson, K. Kaiser, and R. M. W. Amon (2004), Export of young terrigenous dissolved organic carbon from rivers to the Arctic Ocean, *Geophys. Res. Lett.*, *31*, L05305, doi:10.1029/2003GL019251.

Bense, V. F., G. Ferguson, and H. Kooi (2009), Evolution of shallow groundwater flow systems in areas of degrading permafrost, *Geophys. Res. Lett.*, *36*, L22401, doi:10.1029/2009GL039225.

Boyer, E. W., G. M. Hornberger, K. E. Bencala, and D. M. McKnight (1997), Response characteristics of DOC flushing in an alpine catchment, *Hydrol. Process.*, *11*, 1635–1647.

Butman, D., P. A. Raymond, K. Butler, and G. Aiken (2012), Relationships between $\Delta^{14}C$ and the molecular quality of dissolved organic carbon in rivers draining to the coast from the conterminous United States, *Global Biogeochem. Cycles*, *26*, GB4014, doi:10.1029/2012GB004361.

Cory, R. M., M. P. Miller, D. M. McKnight, J. J. Guerard, and P. L. Miller (2010), Effect of instrument-specific response on the analysis of fulvic acid fluorescence spectra, *Limnol. Oceanogr. Methods*, *8*, 67–78.

Davis, J. C., et al. (1990), LLNL/US AMS facility and research program, *Nucl. Instrum.Meth. B*, *52*, 269–272.

Fan, Z., J. C. Neff, and K. P. Wickland (2010), Modeling the production, decomposition, and transport of dissolved organic carbon in boreal soils, *Soil Sci.*, *175*, 223–232, doi:10.1097/ss.0b013e3181e0559a.

Finlay, J., J. Neff, S. Zimov, A. Davydova, and S. Davydov (2006), Snowmelt dominance of dissolved organic carbon in high-latitude watersheds: implications for characterization and flux of river DOC, *Geophys. Res. Lett.*, *33*, L10401, doi:10.1029/2006GL025754.

Frey, K. E., and J. W. McClelland (2009), Impacts of permafrost degradation on arctic river biogeochemistry, *Hydrol. Process.*, *23*, 169–182, doi:10.1002/hyp.7196.

Frey, K. E., and L. C. Smith (2005), Amplified carbon release from vast West Siberian peatlands by 2100, *Geophys. Res. Lett.*, *32*, L09401, doi:10.1029/2004GL022025.

Ge, S., J. McKenzie, C. Voss, and Qingbai W. (2011), Exchange of groundwater and subsurface-water mediated by permafrost response to seasonal and long term air temperature variation, *Geophys. Res. Lett.*, *38*, L14402, doi:10.1029/2011GL047911.

Giesler, R., S. W. Lyon, C.-M. Mörth, J. Karlsson, E. J. Jantze, G. Destouni, and C. Humborg (2014), Catchment-scale dissolved carbon concentrations and export estimates across six subarctic streams in northern Sweden, *Biogeosciences*, *11*, 525–537, doi:10.5194/bg-11-525-2014.

Guo, L., and R. W. Macdonald (2006), Source and transport of terrigenous organic matter in the upper Yukon River: Evidence from isotope ($\delta^{13}C$, $\Delta^{14}C$, and $\delta^{15}N$) composition of dissolved, colloidal, and particulate phases, *Global Biogeochem. Cycles*, *20*, GB2011, doi:10.1029/2005GB002593.

Guo, L., C.-L. Ping, and R. W. Macdonald (2007), Mobilization pathways of organic carbon from permafrost to arctic rivers in a changing climate, *Geophys. Res. Lett.*, *34*, L13603, doi:10.1029/2007GL030689.

Hanley, K. W., W. M. Wolheim, J. Salisbury, T. Huntington, and G. R. Aiken (2013), Controls on dissolved organic carbon quantity and quality in large North American rivers, *Global Biogeochem. Cycles*, *27*, doi:10.1002/gbc.20044.

Harden, J. W., et al. (2012), Field information links permafrost carbon to physical vulnerabilities of thawing, *Geophys. Res. Lett.*, *39*, L15704, doi:10.1029/2012GL051958.

Helms, J. R., A. Stubbins, J. D. Ritchie, E. C. Minor, D. J. Kieber, and K. Mopper (2008), Absorption spectral slopes and slope ratios as indicators of molecular weight, source, and photobleaching of chromophoric dissolved organic matter, *Limnol. Oceanogr.*, *53*, 955–969.

Hicks Pries, C. E. H., E. A. G. Schuur, and K. G. Crummer (2012), Holocene carbon stocks and carbon accumulation rates altered in soils undergoing permafrost thaw, *Ecosystems*, *15*, 162–173, doi:10.1007/s10021-011-9500-4.

Hood, E., J. Fellman, R. G. M. Spencer, P. J. Hernes, R. Edwards, D. D'Amore, and D. Scott (2009), Glaciers as a source of ancient and labile organic matter to the marine environment, *Nature*, *462*, 1044–1048, doi:10.1038/nature08580.

Hornberger, G. M., K. E. Bencala, and D. M. McKnight (1994), Hydrological controls on dissolved organic carbon during snowmelt in the Snake River near Montezuma, Colorado, *Biogeochemistry*, *25*, 147–165.

Hugelius, G., et al. (2013), A new data set for estimating organic carbon storage to 3 m depth in soils of the northern circumpolar permafrost region, *Earth Syst. Sci. Data*, *5*, 393–402, doi:10.5194/essd-5-393-2013.

Jepsen, S. M., C. I. Voss, M. A. Walvoord, J. R. Rose, B. J. Minsley, and B. D. Smith (2013), Sensitivity analysis of lake mass balance in discontinuous permafrost: the example of disappearing Twelve Mile Lake, Yukon Flats, Alaska (USA), *Hydrogeol. J.*, *21*, 185–200.

Jorgenson, M. T., Y. L. Shur, and E. R. Pullman (2006), Abrupt increase in permafrost degradation in Arctic Alaska, *Geophys. Res. Lett.*, *33*, L02503, doi:10.1029/2005GL024960.

Jorgenson, T., K. Yoshikawa, M. Kanevskiy, Y. Shur, V. Romanovsky, S. Marchenko, G. Grosse, J. Brown and B. Jones (2008), Permafrost characteristics of Alaska, in Proceedings of the Ninth International Conference on Permafrost, 121–122, Institute of Northern Engineering, Univ. of Alaska Fairbanks, Fairbanks.

Jorgenson, M. T., et al. (2013), Reorganization of vegetation, hydrology, and soil carbon changes after permafrost degradation across heterogenous boreal landscapes, *Environ. Res. Lett.*, *8*, 035017, doi:10.1088/1748-9326/83/035017.

Kalbitz, K., D. Schwesig, J. Rethemeyer, and E. Matzner (2005), Stabilization of dissolved organic matter by sorption to the mineral soil, *Soil Biol. Biochem.*, *37*, 1319–1331, doi:10.1016/j.soilbio.2004.11.028.

Kanevskiy, M., Y. Shur, B. Connor, M. Dillon, E. Stephani, and J. A. O'Donnell (2012), Study of the ice-rich syngenetic permafrost for road construction (interior Alaska), in *Proceedings of the Tenth International Conference on Permafrost*, pp. 191–196, The Northern Publisher, Salekhard, Russia.

Kawahigashi, M., K. Kaiser, A. Rodionov, and G. Guggenberger (2006), Sorption of dissolved organic matter by mineral soils of the Siberian forest tundra, *Global Change Biol.*, *12*, 1868–1877, doi:10.1111/j.1365-2486.2006.01203.x.

Kicklighter, D. W., D. J. Hayes, J. W. McClelland, B. J. Peterson, A. D. McGuire, and J. M. Melillo (2013), Insights and issues with simulating terrestrial DOC loading of Arctic river networks, *Ecol. Appl.*, *23*, 1817–1836, doi:10.1890/11-1050.1.

Koch, J. C., R. L. Runkel, R. Striegl, and D. M. McKnight (2013), Hydrologic controls on the transport and cycling of carbon and nitrogen in a boreal catchment underlain by continuous permafrost, *J. Geophys. Res. Biogeosci.*, *118*, 698–712, doi:10.1002/jgrg.20058.

Koven, C. D., B. Ringeval, P. Friedlingstein, P. Ciais, P. Cadule, D. Khvorostyanov, G. Krinner, and C. Tarnocai (2011), Permafrost carbon-climate feedbacks accelerate global warming, *Proc. Natl. Acad. Sci. U.S.A.*, *108*, 14,769–14,774, doi:10.1072/pnas.1103910108.

Laudon, H., M. Berggren, A. Agren, I. Buffam, K. Bishop, T. Grabs, M. Jansson, and S. Kohler (2011), Patterns and dynamics of dissolved organic carbon (DOC) in boreal streams: the role of processes, connectivity, and scaling, *Ecosystems*, *14*, 880–893, doi:10.1007/s10021-011-9452-8.

Lyon, S. W., and G. Destouni (2010), Changes in catchment-scale recession flow properties in response to permafrost thawing in the Yukon River Basin, *Int J. Climatol.*, *30*(14), 2138–2145.

Lyon, S. W., M. Morth, C. Humborg, R. Giesler, and G. Destouni (2010), The relationship between subsurface hydrology and dissolved carbon fluxes for a sub-arctic catchment, *Hydrol. Earth Syst. Sci.*, *14*, 941–950, doi:10.5194/hess-14-941-2010.

MacDougall, A. H., C. A. Avis, and A. J. Weaver (2012), Significant contribution to climate warming from the permafrost carbon feedback, *Nat. Geosci.*, *5*, 719–721, doi:10.1038/ngeo1573.

Mann, P. J., A. Davydova, N. Zimov, R. G. M. Spencer, S. Davydov, E. Bulygina, S. Zimov, and R. M. Holmes (2012), Controls on the composition and lability of dissolved organic matter in Siberia's Kolyma River basin, *J. Geophys. Res.*, *117*, G01028, doi:10.1029/2011JG001798.

Mann, W. B. (1983), An international reference material for radiocarbon dating, *Radiocarbon*, *25*(2), 519–527.

Marchenko, S., V. Romanovsky, and G. Tipenko (2008), Numerical modeling of spatial permafrost dynamics in Alaska, in *Proceedings of the Ninth International Conference on Permafrost*, pp. 1125–1130, Institute of Northern Engineering, Fairbanks, Alaska.

McGuire, A. D., et al. (2010), An analysis of the carbon balance of the Arctic Basin from 1997 to 2006, *Tellus B*, *62*, 455–474, doi:10.1111/j.1600-0889.2010.00497.x.

McKnight, D. M., E. W. Boyer, P. K. Westerhoff, P. T. Doran, T. Kulbe, and D. T. Andersen (2001), Spectrofluormetric characterization of dissolved organic matter of precursor organic material and aromaticity, *Limnol. Oceanogr.*, *46*, 34–48.

Murphy, K. R., K. D. Butler, R. G. M. Spencer, C. A. Stedmon, J. R. Boehme, and G. R. Aiken (2010), Measurement of dissolved organic matter fluorescence in aquatic environments: an interlaboratory comparison, *Environ. Sci. Technol.*, *44*, 9405–9412.

Natali, S. M., E. A. G. Schuur, E. E. Webb, C. E. H. Pries, and K. G. Crummer (2013), Permafrost degradation stimulates carbon loss from experimentally warmed tundra, *Ecology*, doi:10.1890/13-0601.1.

Neff, J. C., J. C. Finlay, S. A. Zimov, S. P. Davydov, J. J. Carrasco, E. A. G. Schuur, and A. I. Davydova (2006), Seasonal changes in the age and structure of dissolved organic carbon in Siberian rivers and streams, *Geophys. Res. Lett.*, *33*, L23401, doi:10.1029/2006GL028222.

Nowacki, G., P. Spencer, M. Fleming, T. Brock, and T. Jorgenson (2001), Ecoregions of Alaska, *U.S. Geol. Surv. Open-File Rep.*, 02–297.

O'Donnell, J. A., M. R. Turetsky, J. W. Harden, K. L. Manies, L. E. Pruett, G. Shetler, and J. C. Neff (2009), Interactive effects of fire, soil climate, and moss on CO_2 fluxes in black spruce ecosystems of interior Alaska, *Ecosystems*, *12*, 57–72, doi:10.1007/s10021-008-9206-4.

O'Donnell, J. A., G. R. Aiken, E. S. Kane, and J. B. Jones (2010), Source water controls on the character and origin of dissolved organic matter in streams of the Yukon River basin, Alaska, *J. Geophys. Res.*, *115*, G03025, doi:10.1029/2009JG001153.

O'Donnell, J. A., J. W. Harden, A. D. McGuire, M. Z. Kanevskiy, M. T. Jorgenson, and X. Xu (2011a), The effect of fire and permafrost interactions on soil carbon accumulation in an upland black spruce ecosystem of interior Alaska: implications for post-thaw carbon loss, *Global Change Biol.*, *17*, 1461–1474, doi:10.1111/j.1365-2486.2010.02358.x.

O'Donnell, J. A., J. W. Harden, A. D. McGuire, and V. E. Romanovsky (2011b), Exploring the sensitivity of soil carbon dynamics to climate change, fire disturbance, and permafrost thaw in a black spruce ecosystem, *Biogeosciences*, *8*, 1367–1382, doi:10.5194/bg-8-1367-2011.

O'Donnell, J. A., G. R. Aiken, M. A. Walvoord, and K. D. Butler (2012a), Dissolved organic matter composition of winter stream flow in the Yukon River basin: Implications of permafrost thaw and increased groundwater discharge, *Global Biogeochem. Cycle*, *26*, GB0E06, doi:10.1029/2012GB004341.

O'Donnell, J. A., K. D. Butler, and G. R. Aiken (2012b), Temperature sensitivity of DOC production and transformation in organic soils of the Yukon River basin, Alaska, paper presented at Fall Meeting of the AGU, San Francisco, Calif.

Osterkamp, T. E., L. Viereck, Y. Shur, M. T. Jorgenson, C. Racine, A. Doyle, and R. D. Boone (2000), Observations of thermokarst and its impact on boreal forests in Alaska, USA, *Arct. Antarct. Alp. Res.*, *32*, 303–315.

Pellerin, B. A., J. F. Saraceno, J. B. Shanley, S. D. Sebestyen, G. R. Aiken, W. M. Wolheim, and B. A. Bergamaschi (2011), Taking the pulse of snowmelt: in situ sensors reveal seasonal, event and diurnal patterns of nitrate and dissolved organic matter variability in an upland forest stream, *Biogeochemistry*, *108*, 183–198, doi:10.1007/s10533-011-9589-8.

Petrone, K. C., J. B. Jones, L. D. Hinzman, and R. D. Boone (2006), Seasonal export of carbon, nitrogen and major solutes from Alaskan catchments with discontinuous permafrost, *J. Geophys. Res.*, *111*, G02020, doi:10.1029/2005JG000055.

Poulin, B. A., J. N. Ryan, and G. R. Aiken (2014), Effects of iron on optical properties of dissolved organic matter, *Environ. Sci. Technol.*, doi:10.1021/es502670r.

Raymond, P. A., and J. E. Bauer (2001), Use of ^{14}C and ^{13}C natural abundances for evaluating riverine, estuarine, and coastal DOC and POC sources and cycling: a review and synthesis, *Org. Geochem.*, *32*, 469–485.

Raymond, P. A., and J. E. Saiers (2010), Event controlled DOC export from forested watersheds, *Biogeochemistry*, *100*, 197–209, doi:10.1007/s10533-010-9416-7.

Raymond, P. A., J. W. McClelland, R. M. Holmes, A. V. Zhulidov, K. Mull, B. J. Peterson, R. G. Striegl, G. R. Aiken, and T. Y. Gurovaya (2007), Flux and rate of dissolved organic carbon exported to the Arctic Ocean: A carbon isotopic study of the fiver largest arctic rivers, *Global Biogeochem. Cycles*, *21*, GB4011, doi:10.1029/2007GB002934.

Raymond, P. A., et al. (2013), Global carbon dioxide emissions from inland waters, *Nature*, *503*, 355–359, doi:10.1038/nature12760.

Roach, J., B. Griffith, D. Verbyla, and J. Jones (2011), Mechanisms influencing changes in lake area in Alaskan boreal forest, *Global Change Biol.*, *17*, 2567–2583, doi:10.1111/j.1365-2486.2011.02446.x.

Romanovsky, V. E., S. L. Smith, and H. H. Christiansen (2010), Permafrost thermal state in the polar northern hemisphere during the International Polar Year 2007–2009: A synthesis, *Permafrost Periglac.*, *21*, 106–116, doi:10.1002/ppp.689.

Schaefer, K., H. Lantuit, V. E. Romanovsky, and E. A. G. Schuur (2012), Policy implications of warming permafrost, United Nations Environment Programme.

Schuur, E. A. G., et al. (2008), Vulnerability of permafrost carbon to climate change: implications for the global carbon cycle, *BioScience*, *58*, 701–714.

Spencer, R. G. M., G. R. Aiken, K. P. Wickland, R. G. Striegl, and P. J. Hernes (2008), Seasonal and spatial variability in dissolved organic matter quantity and composition from the Yukon River basin, Alaska, *Global Biogeochem. Cycles*, *22*, GB4002, doi:10.1029/2008GB003231.

Spencer, R. G. M., G. R. Aiken, K. D. Butler, M. M. Dornblaser, R. G. Striegl, and P. J. Hernes (2009), Utilizing chromophoric dissolved organic matter measurements to derive export and reactivity of dissolved organic carbon exported to the Arctic Ocean: A case study of the Yukon River, Alaska, *Geophys. Res. Lett.*, *36*, L06401, doi:10.1029/2008GL036831.

Spencer, R. G. M., G. R. Aiken, R. Y. Dyda, K. D. Butler, B. A. Bergamaschi, and P. J. Hernes (2010), Comparison of XAD with other dissolved lignin isolation techniques and a compilation of analytical improvements for the analysis of lignin in aquatic settings, *Org. Geochem.*, *41*, 445–453, doi:10.1016/j.orggeochem.2010.02.004.

Spencer, R. G. M., K. D. Butler, and G. R. Aiken (2012), Dissolved organic carbon and chromophoric dissolved organic matter properties of rivers in the USA, *J. Geophys. Res.*, *117*, G03001, doi:10.1029/2011JG001928.

Striegl, R. G., G. R. Aiken, M. M. Dornblaser, P. A. Raymond, and K. P. Wickland (2005), A decrease in discharge-normalized DOC export by the Yukon River during summer through autumn, *Geophys. Res. Lett.*, *32*, L21413, doi:10.1029/2005GL024413.

Striegl, R. G., M. M. Dornblaser, G. R. Aiken, K. P. Wickland, and P. A. Raymond (2007), Carbon export and cycling by the Yukon, Tanana, and Porcupine rivers, Alaska, 2001–2005, *Water Resour. Res.*, *43*, W02411, doi:10.1029/2006WR005201.

Striegl, R. G., M. M. Dornblaser, C. P. McDonald, J. R. Rover, and E. G. Stets (2012), Carbon dioxide and methane emissions from the Yukon River system, *Global Biogeochem. Cycles*, *26*, GB0E05, doi:10.1029/2012GB004306.

Stuiver, M., and H. A. Polach (1977), Discussion: reporting of ^{14}C data, *Radiocarbon*, *19*, 355–363.

Tank, S. E., K. E. Frey, R. G. Striegl, P. A. Raymond, R. M. Holmes, J. W. McClelland, and B. J. Peterson (2012), Landscape-level controls on dissolved carbon flux from diverse catchments of the circumboreal, *Global Biogeochem. Cycles*, *26*, GB0E02, doi:10.1029/2012GB004299.

Tarnocai, C., J. G. Canadell, E. A. G. Schuur, P. Kuhry, G. Mazhitova, and S. Zimov (2009), Soil organic carbon pools in the northern circumpolar permafrost region, *Global Biogeochem. Cycles*, *23*, GB2023, doi:10.1029/2008GB003327.

Trumbore, S. E., and J. W. Harden (1997), Accumulation and turnover of carbon in organic and mineral soils of the BOREAS northern study area, *J. Geophys. Res.*, *102*(D24), 28,817–28,830, doi:10.1029/97JD02231.

Vogel, J. S., J. R. Southon, and D. E. Nelson (1987), Catalyst and binder effects in the use of filamentous graphite for AMS, *Nucl. Instrum. Methods Phys. Res., Sect. B*, *29*, 50–56.

von Deimling, T. S., M. Meinshausen, A. Levermann, V. Huber, K. Frieler, D. M. Lawrence, and V. Brovkin (2012), Estimating the near-surface permafrost-carbon feedback on global warming, *Biogeosciences*, *9*, 649–665, doi:10.5194/bg-9-649-2012.

Vonk, J. E., and O. Gustafsson (2013), Permafrost-carbon complexities, *Nat. Geosci.*, *6*, 675–676, doi:10.1038/ngeo1937.

Vonk, J. E., et al. (2012), Activation of old carbon by erosion of coastal and subsea permafrost in Arctic Siberia, *Nature*, *489*, 137–140, doi:10.1038/nature11392.

Vonk, J. E., et al. (2013), High biolability of ancient permafrost carbon upon thaw, *Geophys. Res. Lett.*, *40*, 2689–2693, doi:10.1002/grl.50348.

Walvoord, M. A., and R. G. Striegl (2007), Increased groundwater to stream discharge from permafrost thawing in the Yukon River basin: Potential impacts on lateral export of carbon and nitrogen, *Geophys. Res. Lett.*, *34*, L12402, doi:10.1029/2007GL030216.

Walvoord, M. A., C. I. Voss, and T. P. Wellman (2012), Influence of permafrost distribution on groundwater flow in the context of climate-driven permafrost thaw: Example from Yukon Flats Basin, Alaska, USA, *Water Resour. Res.*, *48*, 7, doi:10.1029/2011WR011595.

Weishaar, J. L., G. R. Aiken, B. A. Bergamaschi, M. S. Fram, R. Fujii, and K. Mopper (2003), Evaluation of specific ultraviolet absorbance as an indicator of the chemical composition and reactivity of dissolved organic carbon, *Environ. Sci. Technol.*, *37*, 4702–4708, doi:10.1021/es030360x.

Wellman, T., C. Voss, and M. Walvoord (2013), Impacts of climate, lake size, and supra- and sub-permafrost groundwater flow on lake-talik evolution, Yukon Flats, Alaska, USA, *Hydrogeol. J.*, *21*, 281–298, doi:10.1007/s10040-012-0941-4.

Wickland, K. P., G. R. Aiken, K. Butler, M. M. Dornblaser, R. G. M. Spencer, and R. G. Striegl (2012), Biodegradability of dissolved organic carbon in the Yukon River and its tributaries: Seasonality and importance of inorganic nitrogen, *Global Biogeochem. Cycles*, *26*, GB0E03, doi:10.1029/2012GB004342.

Yoshikawa, K., W. R. Bolton, V. E. Romanovsky, M. Fukuda, and L. D. Hinzman (2003), Impacts of wildfire on the permafrost in the boreal forests of Interior Alaska, *J. Geophys. Res.*, *108*(D1), 8148, doi:10.1029/2001JD000438.